Proceedings of the ASME 2020
International Design Engineering Technical Conferences
and Computers and Information in Engineering Conference
IDETC/CIE2020
August 16-19, 2020, St. Louis, MO, USA

IDETC2020-22668

PREDICTIVE HUMAN-IN-THE-LOOP SIMULATIONS FOR ASSISTIVE EXOSKELETONS

Xianlian Zhou[1]
New Jersey Institute of Technology
Newark, NJ

ABSTRACT

Design and evaluation of exoskeletons is often a time consuming and costly process that involves prototyping, human testing, and multiple design iterations. For active exoskeletons, the primary challenge is to detect the wearer's movement intent and provide potent assistance, which often requires sophisticated control algorithms. The goal of this study is to integrate human musculoskeletal models with robot modeling and control for virtual human-in-the-loop evaluation of exoskeleton design and control. We present potential strategies for assisting various human motions such as squatting, lifting, walking, and running. Several exoskeleton designs (for back, upper extremity, and lower extremity) and their control methods are evaluated with an integrated human-in-the-loop simulation approach to study their functionalities and biomechanical effects on the wearer' musculoskeletal system. We hope this simulation paradigm can be utilized for virtual design and evaluation of exoskeletons and pave the way to build or optimize exoskeletons.

Keywords: Neck, musculoskeletal model, head supported mass, walking and running

NOMENCLATURE

DOF	degree of freedom
GRF	ground reaction force
MSK	musculoskeletal

1. INTRODUCTION

Wearable exoskeletons or exosuits are becoming a new frontier of interdisciplinary research in robotics and biomechanics. The main objectives of wearable exoskeletons are to augment human performance, assist human motions to reduce fatigue or prevent injuries, or assist with disabilities for rehabilitation. Many exoskeletons or exosuit systems have been developed in recent years. Early efforts can date back to 1960s' General Electric HARDIMAN project which attempted to develop the first practical powered exoskeleton for military applications. Other US military sponsored exoskeletons include the Berkeley Bionics/Lockheed Martin HULC (Human Universal Load Carrier) system and the SARCOS Labs/Raytheon XOS system. Outside the US, similar efforts have also been conducted and resulted in several exoskeleton systems for civilian or military applications such as the French RB3D's HERCULES system and the Japanese Cyberdyne's HAL system [1]. In addition to rigid-component robotic exoskeleton systems, soft exosuits [2] were also introduced aiming to provide gait assistance and reduce metabolic cost of human locomotion. Compared to conventional robotic exoskeletons, exosuit is in general more lightweight but provides limited power assistance.

A well-designed control and actuation scheme is particularly important for any exoskeleton due to its interaction with human and safety concerns. However, this is a challenging task due to the complexity and variability of human locomotion. The HAL system utilizes surface EMG and a walking pattern based control system to determine user intent and operate the suit. However, it was reported to take two months to optimally calibrate the system for a specific user [1]. The BLEEX (Berkeley Lower Extremity Exoskeleton) system developed by Kazerooni et al. [3] utilizes sensory information from the exoskeleton and enables the exoskeleton to balance on its own while the human wearer provides a forward interaction force to guide the system during walking. Many other control and actuation approaches have also be present in the literature [4, 5].

One big challenge of robotic exoskeleton design and control is to evaluate its effects on human body. Most researchers have focused on evaluating exoskeletons' effects on wearers' metabolic cost. A recent US army experimental study conducted

[1] Contact author: alexzhou@njit.edu

by Gregorczyk et al. [6] evaluated a prototype exoskeleton system similar to HULC and found that the system altered the wearers' gait and increased their oxygen consumption (VO2) significantly. Zhang et al. [7] developed a method to identify assistance profiles of an ankle exoskeleton that minimizes human energy cost during walking using human-in-the-loop testing and indirect calorimetry measurement of metabolic rates. Optimized torque patterns from an exoskeleton worn on one ankle was shown to be able to reduce metabolic rates by over 20%. Similarly, Ding et al. [8] used a human-in-the-loop testing method to optimize hip assistance of a soft exosuit during walking and observed around 17% of metabolic cost reduction. However, such evaluation cannot give direct clues on the effects of exoskeletons on musculoskeletal (MSK) loadings (muscle, ligament, disc or joint reaction forces). Unfortunately, there are no direct, non-invasive measurements of the MSK forces, which renders experimental evaluation of exoskeletons less useful in this regard.

Due to the challenges in design, control, and evaluation of exoskeleton systems, it is highly desired to virtually test a prototype system before manufacturing and assembly in order to save material cost and labor. This requires a human-in-the-loop modeling method to simulate exoskeleton-wearer interaction, as demonstrated in several recent studies. For example, Zhou et al. [9] used AnyBody® for design and optimization of a spring-loaded cable-driven robotic exoskeleton. Koller et al. [10] used OpenSim to study adaptive gain proportional myoelectric controllers for a robotic ankle exoskeleton. Petric et al. [11] introduced a novel control framework for an arm exoskeleton that takes into account force of the human arm. Recently, Delp's group reported two studies on simulating ideal assistive devices to reduce the metabolic cost of walking [12] and running [13]. In both studies, OpenSim was used to generate muscle-driven simulations of subjects walking or running with massless assistive devices, which applied idealized net joint moments or torques directly to the human joints without considering physical interaction forces between the devices and the subjects. In their simulations, the kinematics and the ground reaction forces (GRFs) that were measured experimentally during unassisted running were used for tracking control.

The goal of this study is to integrate high fidelity human musculoskeletal models with robot modeling and control for human-in-the-loop evaluation of exoskeleton design and control. We will present potential strategies for assisting various human motions such as squatting, lifting, walking, and running. Several exoskeleton designs (for back, upper extremity, and lower extremity) and their control methods will be evaluated with an integrated human-in-the-loop simulation approach to study their functionalities and biomechanical effects on the wearer' MSK system. With such an integrated evaluation framework, the cause-effect relationships can be evaluated by varying exoskeleton assistance and examining its effects on human MSK loadings.

2. MATERIALS AND METHODS

2.1 Musculoskeletal models

In this study, we employed several MSK models that have been developed by different groups over the years. For example, the lumbar model developed by Christophy et al. [14] and the lower leg muscle model from Hamner et al. [15], and the upper extremity model developed by Saul et al. [16]. These models will later be introduced and integrated with different exoskeletons for human-in-the-loop simulations.

2.2 Modeling of Exoskeleton and Human Interaction

The human and exoskeleton are often tied together with elastic straps. Modeling the straps is challenging because they are soft and deformable. Previously, we have developed a detailed model of strap as multi-segment elastic band as shown in Fig. 1a. This strap model checks the contact between the band and the human body to avoid penetration and maintain its proper shape through wrapping around contact objects. However, this approach is relatively complicated and less efficient for human-exoskeleton simulations. A simplified approach is to model the strap as a direction-dependent spring-damper that connect corresponding anchor points on the body and exoskeleton as displayed in Fig 1b-c. In this setup, the stiffness of a strap in the movement direction can be assumed to be many times of the stiffness in the sliding or soft constraint direction.

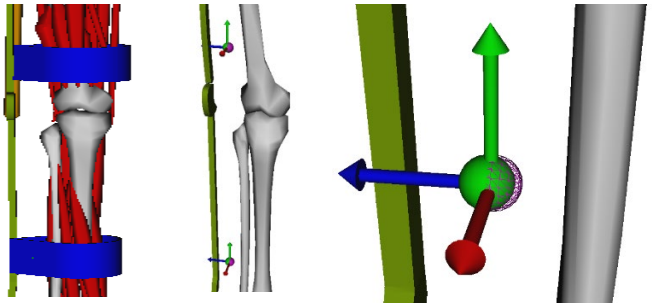

(a) (b) (c)

FIGURE 1: (a) Elastic band model of straps between the leg and exoskeleton; (b) Straps modeled as tri-directional force elements between corresponding anchor points. (c) Zoom-in view of the tibia force element with the green sphere anchored on the exoskeleton and the purple wire sphere anchored on the human body.

To model the physical interaction forces between the human and exoskeleton, we introduced a tri-directional spring-damper force element that mimics the contact or constraint between them. The tri-directional force element was introduced by connecting two corresponding anchor points on the body and exoskeleton, as shown in Fig. 1c, to capture the relative movement between these points. The force element computes three (XYZ) directional distances and generates (either positive or negative) forces along these directions during their relative movements. At the initial assembly, these two points are coincident to each other and generate zero force ($x_0 = y_0 = z_0 = 0$). The forces generated by the force element were modeled by linear damped springs:

$$\begin{cases} f_x = k_x(x - x_0) + c_x\dot{x} \\ f_y = k_y(y - y_0) + c_y\dot{y} \\ f_z = k_z(z - z_0) + c_z\dot{z} \end{cases} \quad (1)$$

The stiffness and damping constants of the directional force element can be calibrated with experimental data. The tri-directional force element can be easily extended to a 6-direction force element such that two opposite directions along one axis can have different stiffnesses.

2.3 Simulation methods

An integrated human-exoskeleton model can be treated a unified multibody system governed by the following dynamics equations:

$$\boldsymbol{M}(\boldsymbol{q})\ddot{\boldsymbol{q}} + \boldsymbol{c}(\boldsymbol{q}, \dot{\boldsymbol{q}}) = \boldsymbol{\tau} + \boldsymbol{J}^T\boldsymbol{F} + \sum_{\boldsymbol{m}} \boldsymbol{J}_{\boldsymbol{m}}^T \boldsymbol{f}_{\boldsymbol{m}},$$
$$\boldsymbol{g}(\boldsymbol{q}, \dot{\boldsymbol{q}}) = \boldsymbol{0}, \quad (2)$$

where $\boldsymbol{q}$, $\dot{\boldsymbol{q}}$ and $\ddot{\boldsymbol{q}}$ denote the generalized coordinates of assembled system, their velocities and accelerations, $\boldsymbol{M}(\boldsymbol{q})$ is the generalized inertia matrix, $\boldsymbol{c}(\boldsymbol{q}, \dot{\boldsymbol{q}})$ is the Coriolis and gravitational forces, τ is the generalized (external) joint torques. $\boldsymbol{g}$ denotes constraint functions and $\boldsymbol{J}$ is its Jacobian. $\boldsymbol{F}$ is the constraint or interaction forces or Lagrange multipliers that will be solved together with generalized acceleration $\ddot{\boldsymbol{q}}$. $\boldsymbol{J}_{\boldsymbol{m}}^{\boldsymbol{T}}$ is the Jacobian matrix that maps each a muscle force f_m to a generalized joint torque vector.

With the developed model and simulated controlled framework, we can perform computer simulations to study the co-operation between human and exoskeleton. All simulations in this study were performed with an in-house extended version of the musculoskeletal simulation code, CoBi-Dyn, initially developed at CFD Research Corporation (Huntsville, AL). A hybrid inverse dynamics (ID) and forward dynamics (FD) simulation framework similar to the one presented in [17] was employed. Some joints were classified as ID joints such that their motions can be prescribed to track an input motion whereas others were classified as FD joints such that their motions were driven by the actuation or interaction forces. At each time step, the hybrid dynamics framework predicted joint torques for all ID joints and accelerations for FD joints. The predicted ID joint torques were the target or desired torques that ideally shall be generated from muscles spanning these joints. To compute muscle forces, one of the goals was to find a feasible muscle force combination that contributed to generate the desired joint torques as closely as possible. Due to the redundancy of the muscles, there could be many such combinations and thus muscle forces were determined by solving an optimization problem. The final objective of this optimization problem was to minimize an objective function, defined as

$$\sum_{i=1}^{n} \left(\frac{f_i}{f_i^{max}}\right)^p + w\boldsymbol{C}^T\boldsymbol{C} \quad (1)$$

where f_i was the force of the ith muscle, f_i^{max} was the maximum attainable muscle force at its current state, $\boldsymbol{C}$ was the difference vector between the desired joint moments and the moments generated by spanning muscles ($\boldsymbol{C}$ is often called the residual torque), w was a weighting or penalty factor, and $\frac{f_i}{f_i^{max}}$ can be considered as the muscle activation or effort for simplicity, and p is the polynomial order of the muscle effort. In the simulations below, $p = 2$ was chosen based on review of literature in [18], and $w = 100$ were used as penalty factor for moment differences. Since moment differences are typically much larger than the square of muscle activation, the use of 100 is reasonable. In fact, use of a larger penalty factor did not affect our simulation results.

3. RESULTS AND DISCUSSION

3.1. Simulation of a spine-inspired exoskeleton

Previously, we have modeled a novel continuum, spine-inspired soft exoskeleton [19]. This exoskeleton has a unique feature of generating a perpendicular assistance force to the back during lifting. On the contrary, there are some muscle-inspired spine exoskeletons that generate spine-parallel assistance forces similar to erector spinae muscles. In this study, we conducted simulations to illustrate the differences in assistance of these two design concepts. A highly detailed lumbar musculoskeletal model [14] was integrated with a generic full body model for this study. The model contains 5 flexible L1-L5 lumbar spine joints with predefined lordosis constraint and over 200 muscles around torso and lumbar regions. For simplicity, we did not explicitly model the exoskeleton and its interactions with the human. Instead, idealized assistance forces were directly applied to a location on the back. The exoskeleton assistance force starts with its maximum value of 250N at the beginning (fully bended posture) and gradually decreased to zero at the end (4 seconds, standing upright posture), following a cosine profile. The direction of the force was switched from perpendicular to parallel when simulating the muscle-inspired exoskeleton, as shown in Fig. 2a. In Fig. 2b, the muscle generated torques at the L5-S1 level and the total force of the erector spinae muscles are shown for three cases: unassisted, assisted with a parallel force, and assisted with a perpendicular force. In Fig. 2c, the comparison of joint reaction forces (compression and shear) for parallel and perpendicular assistances are shown. Clearly, it can be observed both exoskeleton assistance methods reduce MSK loading substantially; the spine-inspired exoskeleton reduces the maximum compressive and shear forces nearly by 40% and perform much better than the muscle-inspired exoskeleton.

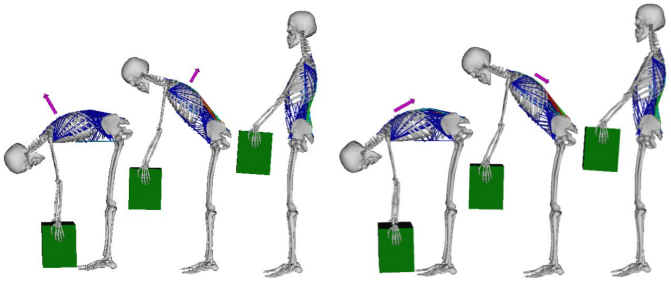

(a)

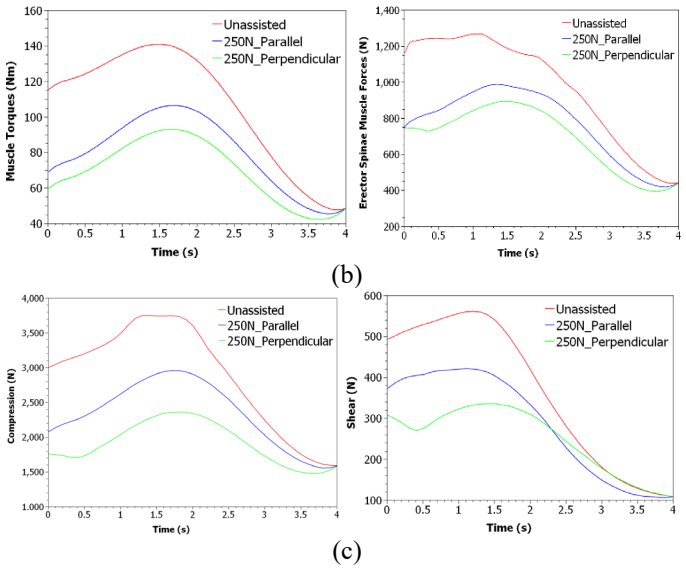

FIGURE 2: (a) Simulations of applying perpendicular (spine-inspired) and parallel (muscle-inspired) assistance force profiles to the back during lifting. The purple arrows are the assistance forces. The color of muscle indicates its activation level with red being the highest (1) and blue being the lowest (0); (b) The two curve plots show comparison of the muscle generated spine joint torques and total forces of the erector spinae muscles; (c) The two curve plots show the comparison of joint reaction forces (compression and shear) for parallel and perpendicular assistances.

3.2. Simulation of idealized hip assistance to squatting and walking

Exoskeleton hip assistance during walking has been studied by multiple research groups [8, 12] while hip assistance during squatting has not been well studied. To help evaluate the effects of hip assistance during these two activities, we conducted numerical simulations of idealized hip torque assistance without explicitly modeling the exoskeleton. The hip assistance torques are assumed to be proportional to the total muscle hip torques required without exoskeleton and 30% assistance was employed in the simulations. The squat cycle (down and up) is 4 seconds and the walking cycle is about 1.21 seconds. The walking motion and GRF data were obtained from a motion capture experiment, whereas the symmetric squatting motion was synthesized from a squatting video and GRFs were predicted with four contact points defined on each foot. In both simulations, the predefined motions were tracked with muscle generated torques. As shown in Fig. 3b, squatting requires higher quadriceps (rectus femoris) muscle activation and higher total metabolic rate of muscles than walking, and the reduction in both activations and metabolic rates due to hip assistance can be clearly observed for both activities. The metabolic rate was computed based on muscle energetics model from [20] with modification from [21].

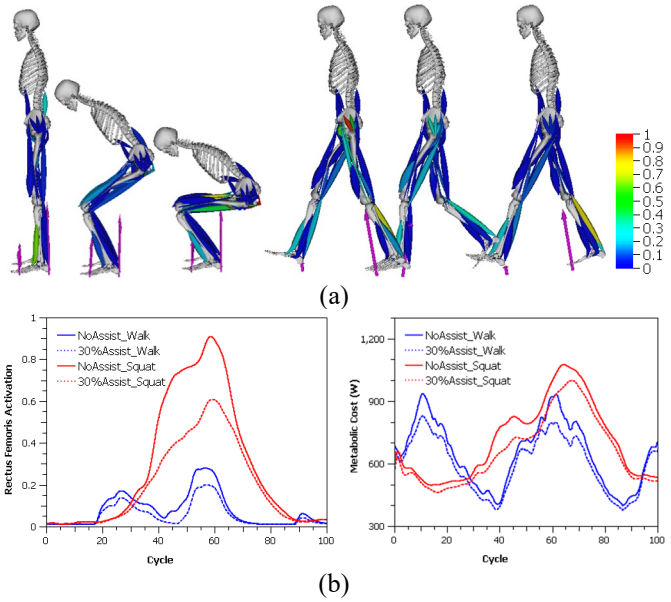

FIGURE 3: (a) Simulations of squatting and walking. The purple arrows are the ground reaction forces and the color of the muscle indicates the activation level. (b) The two plots show the reduction of rectus femoris muscle activations and total muscle metabolic rates under 30% hip torque assistance.

3.3. Controller evaluation for a lower extremity exoskeleton

In this study, we use the integrated human-in-the-loop simulation paradigm for design and evaluation of a lower extremity exoskeleton that is elastically strapped onto human lower limbs. The exoskeleton, shown in Fig. 4a, has 3 rotational DOFs (degrees of freedom) on each side and weights 23kg. It contains 6 idealized actuators (displayed as yellow cylinders) that can generate both positive and negative (or push and pull) forces. These idealized actuators can mimic typical hydraulic actuators or electric motor actuators and they are attached at proper locations of the mechanical parts to allow actuation of each joint along their DOF. Each actuator can generate an active force up to $\pm 4000N$ (positive: pull; negative: push), achievable by many hydraulic or electric motor actuators. The exoskeleton was assembled onto a human body musculoskeletal (MSK) model with elastic straps on the legs (Fig. 4a). And the load support (top part) was assumed to be tied to the human body such that there is no relative movement.

Without a physical exoskeleton prototype, experimental measurements of wearer's motions, GRFs and other interaction forces between exoskeleton and wearer were not available. Nonetheless, such data were readily available for normal motion (without exoskeleton) from motion capture experiments. Considering this, we assumed the wearer was capable of maintain his/her normal gait (with increased or decreased effort) when wearing a properly designed exoskeleton, possibly after training. Consequently, the measured normal motion can be used as the target motion for exoskeleton involved simulations. However, the GRFs measured from normal gaits are not directly applicable to exoskeleton simulations due to the weight

difference. Therefore, the GRFs must be predicted in these simulations. In this study, a running motion was utilized due to the relative simplicity and accuracy in predicting GRFs. Unlike a walking motion that has a double stance phase, running has only two phases: a single supporting phase and a flying phase. GRF prediction is only needed for the single supporting phase and it can be estimated through an equivalent force transformation method or an optimization method minimizing the difference between GRF and equivalent force with proper friction constraints [22]. The running motion data utilized in this study was collected in a study by Hamner et al [15]. The subject with weight of 65.9kg ran at 3.96m/s (14.26km/h), three times his self-selected walking speed. With the assembled exoskeleton, the total weight is 88.9kg.

We first performed a running simulation with straps modeled as multi-segment elastic bands. The stretch of the straps is shown in the right figure of Fig 4a. However, due to difficulty in tuning the elastic material properties of these strap bands, we found it is hard to generate smooth interaction forces on the body that consequently affects the controller evaluation negatively. Therefore, we opted to use the simpler tri-direction spring force elements to model the interaction forces. The femur straps were assumed to have different directional force responses for relative XYZ movements between the exo-femur and human femur (X: fore-aft, Y: vertical, Z: lateral). So are the tibia straps. It enables setup of strong resistance against relative movement along the fore-aft direction and much weaker resistance along the vertical (sliding) and lateral (abduction/adduction) directions. This setup allows simulation of straps made of partial metal or other hard materials (e.g. at the front and back sides of the leg) and partial elastic fabric (e.g. at the inner side of the leg). The stiffness and damping constants of the four directional force elements are listed in Table 1.

We designed two torque compensation controllers for the exoskeleton: one aims to reduce interference (control 1) and the other (control 2) aims to provide maximum assistance to human motions, respectively. The details of the torque controllers can be found in [23]. These two torque controllers were virtually evaluated through numerical simulations of running. In Fig. 4b, snapshots of the simulation with the control 2 are shown. In Fig. 4c, the femur and tibia spring forces along the fore-aft direction are shown for all three cases: passive exoskeleton, active exoskeleton with control 1, and active exoskeleton with control 2. The spring forces for control 1 largely follow the same pattern as the passive exoskeleton but with much smaller magnitude, indicating less interference from exoskeleton to the wearer. In a wide range of the gait cycle, the spring forces from control 2 have opposite signs from the passive exoskeleton or control 1, which clearly indicates active assistance instead of interference is given to human motion. Comparing muscle activations for the controller 2 case with other cases, we observed reductions of muscle activations in most muscles. Due to changes in muscle contractions, the joint reaction forces varied accordingly. The predicted joint forces for passive exoskeleton and active control 1 are both significantly higher than those of normal running whereas the control 2 reduces the peak force significantly but is still greater than that of normal running, which can be attributed to the added weight from the exoskeleton despite the torque assistance it provides.

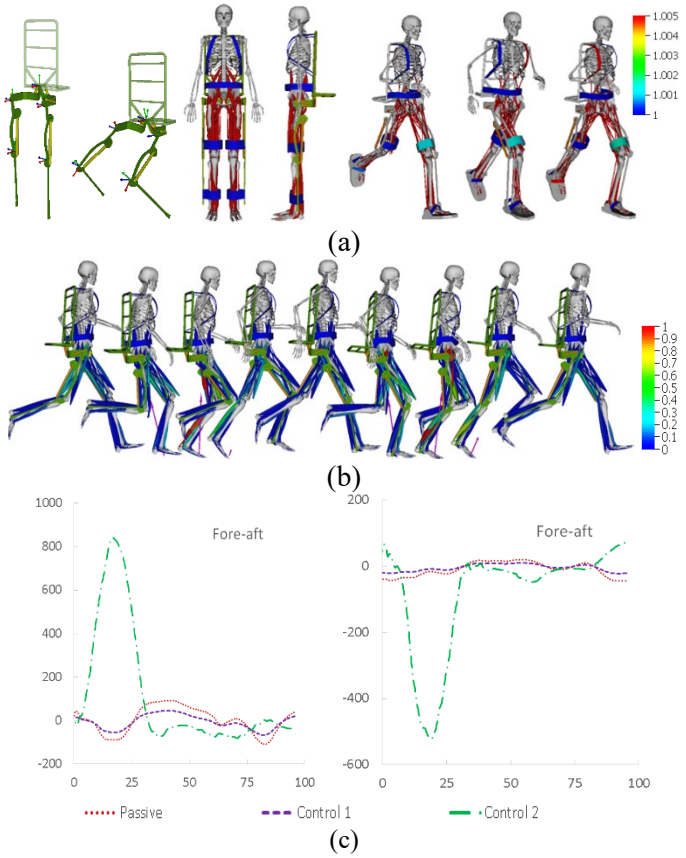

FIGURE 4: (a) Left: the lower extremity exoskeleton assembled onto the human body. Right: prediction of strap stretch (colored) and forces during human-exoskeleton interaction. (b) Simulation of a running gait cycle with the powered exoskeleton employing a toque compensation controller (control 2). The exoskeleton parts are rendered in green and the linear actuators are rendered in gold. The muscle color indicates its activation, and purple arrows are the predicted GRFs. (c) Femur (left) and tibia (right) spring forces along the fore-aft direction.

TABLE 1. Stiffness and damping of the direction springs.

Directional springs	Stiffness (N/m)			Damping (Ns/m)		
	k_x	k_y	k_z	c_x	c_y	c_z
Femur	160000	1600	1600	400	40	40
Tibia	160000	1600	1600	400	40	40

3.4. Simulation of lifting with exoskeleton

Our predictive human-in-the-loop simulation framework can be utilized to study lifting with an upper extremity exoskeleton. In Fig. 5, a simulation of box lifting with a mock upper extremity exoskeleton system similar to the commercial EksoVest system is shown. The system provides joint torques within an assistance zone, defined as the shoulder elevation angle between -40° to 40°. A linear torque assistance profile was assumed to start from zero at -40° and gradually increases

to the maximum of $10Nm$ at 0°, at which point the box might be further away from the shoulder and generate the largest moment at the shoulder joint. Then the torque linearly decreased again to zero at the highest angle of 40°. During the simulation (shown in Fig. 5b), the arm joints tracked an experimentally captured motion (without exoskeleton) under the influence of active assistance from the exoskeleton. For comparison, we also simulated the same motion with the exoskeleton in a passive mode (no assistance provided). In Fig 6, comparisons of muscle generated torques and average muscle activations are shown for both cases. It clearly shows the reduction in both the joint torques and the muscle activations due to the assistance provided.

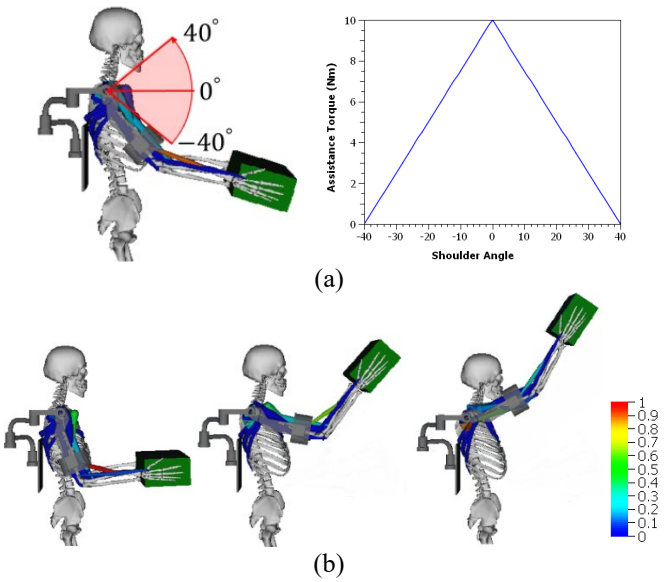

FIGURE 5: (a) Integration of an upper extremity musculoskeletal model [16] with a mock exoskeleton system (similar to EksoVest, https://eksobionics.com/eksoworks/eksovest/), which provides assistance torques during the shoulder angle activated assistance zone. (b) Simulation of a box lifting motion with the assistance from the exoskeleton. The muscle color shows its activation.

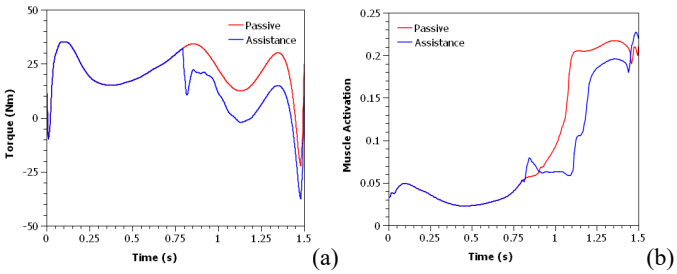

FIGURE 6: (a) Comparison of shoulder muscle generated torques for the passive and active exoskeletons; (b) Comparison of average muscle activation (normalized) for the passive and active exoskeletons.

4. CONCLUSION

In this work, we presented a predictive human-in-the-loop simulation paradigm for active exoskeleton evaluation. Human musculoskeletal models were integrated with robot models for virtual human-in-the-loop evaluation of exoskeleton design and control. Several exoskeleton designs (for back, upper extremity, and lower extremity) and their assistances to various human motions such as squatting, walking, running, and lifting were demonstrated. Different control methods were evaluated to study their functionalities and biomechanical effects on the wearer' musculoskeletal system. By examining the interaction forces, human joint torques and joint reaction forces, and by comparing them with those from the pure passive exoskeleton, our simulations have provided sound evidence of the efficacy of different assistance profiles or control methods. In the future, parametric simulations can also be performed to further optimize design and control parameters. In addition, experimental studies with physical exoskeletons shall be performed to validate the simulated results. In summary, the presented simulation paradigm can be utilized for virtual design and evaluation of exoskeletons and pave the way to build optimized exoskeleton prototypes for experimental evaluation.

REFERENCES

[1] E. Guizzo and H. Goldstein, "The rise of the body bots," *Ieee Spectrum,* vol. 42, no. 10, p. 42, 2005.

[2] M. Wehner *et al.*, "A lightweight soft exosuit for gait assistance.," pp. 3362--3369, 2013.

[3] H. Kazerooni, J. L. Racine, L. H. L. Huang, and R. Steger, "On the Control of the Berkeley Lower Extremity Exoskeleton (BLEEX)," *Proceedings of the 2005 IEEE International Conference on Robotics and Automation,* 2005.

[4] H. Herr, "Exoskeletons and orthoses: classification, design challenges and future directions," *Journal of NeuroEngineering and Rehabilitation,* vol. 6, no. 1, p. 21, 2009.

[5] D. P. Ferris and C. L. Lewis, "Robotic lower limb exoskeletons using proportional myoelectric control," pp. 2119--2124, 2009.

[6] K. N. Gregorczyk, L. Hasselquist, J. M. Schiffman, C. K. Bensel, J. P. Obusek, and D. J. Gutekunst, "Effects of a lower-body exoskeleton device on metabolic cost and gait biomechanics during load carriage.," *Ergonomics,* vol. 53, no. 10, pp. 1263--1275, 2010.

[7] J. Zhang *et al.*, "Human-in-the-loop optimization of exoskeleton assistance during walking," *Science,* vol. 356, no. 6344, pp. 1280-1284, 2017.

[8] Y. Ding, M. Kim, S. Kuindersma, and C. J. Walsh, "Human-in-the-loop optimization of hip assistance with a soft exosuit during walking," *Science Robotics,* vol. 3, no. 15, p. eaar5438, 2018.

[9] L. Zhou, S. Bai, M. S. Andersen, and J. Rasmussen, "Modeling and design of a spring-loaded, cable-driven, wearable exoskeleton for the upper extremity," *Modeling, Identification and Control,* vol. 36, no. 3, pp. 167--177, 2015.

[10] J. R. Koller, D. A. Jacobs, D. P. Ferris, and C. D. Remy, "Learning to walk with an adaptive gain proportional

myoelectric controller for a robotic ankle exoskeleton," *Journal of neuroengineering and rehabilitation,* vol. 12, no. 1, p. 97, 2015.
[11] T. Petric, L. Peternel, J. Morimoto, and J. Babic, "Assistive arm-exoskeleton control based on human muscular manipulability," *Frontiers in neurorobotics,* vol. 13, p. 30, 2019.
[12] C. L. Dembia, A. Silder, T. K. Uchida, J. L. Hicks, and S. L. Delp, "Simulating ideal assistive devices to reduce the metabolic cost of walking with heavy loads," *PloS one,* vol. 12, no. 7, p. e0180320, 2017.
[13] T. K. Uchida, A. Seth, S. Pouya, C. L. Dembia, J. L. Hicks, and S. L. Delp, "Simulating ideal assistive devices to reduce the metabolic cost of running," *PloS one,* vol. 11, no. 9, p. e0163417, 2016.
[14] M. a. S. Christophy, Nur Adila Faruk and Lotz, Jeffrey C and O'Reilly, Oliver M, "A musculoskeletal model for the lumbar spine," vol. 11, ed. Biomechanics and modeling in mechanobiology: Springer, 2012, pp. 19--34.
[15] S. R. Hamner, A. Seth, and S. L. Delp, "Muscle contributions to propulsion and support during running.," *Journal of biomechanics,* vol. 43, no. 14, pp. 2709--16, 2010.
[16] K. R. Saul *et al.*, "Benchmarking of dynamic simulation predictions in two software platforms using an upper limb musculoskeletal model," *Computer methods in biomechanics and biomedical engineering,* vol. 18, no. 13, pp. 1445-1458, 2015.
[17] X. Zhou, P. Whitley, and A. Przekwas, "A Musculoskeletal Fatigue Model for Prediction of Aviator Neck Maneuvering Loadings," *International Journal of Human Factors Modelling and Simulation,* vol. 4, no. 3-4, pp. 191--219, 2014.
[18] A. Erdemir, S. McLean, W. Herzog, and A. J. van den Bogert, "Model-based estimation of muscle forces exerted during movements.," *Clinical biomechanics (Bristol, Avon),* vol. 22, no. 2, pp. 131--154, 2007.
[19] X. Yang *et al.*, "Spine-inspired continuum soft exoskeleton for stoop lifting assistance," *IEEE Robotics and Automation Letters,* vol. 4, no. 4, pp. 4547-4554, 2019.
[20] B. R. Umberger, K. G. M. Gerritsen, and P. E. Martin, "A model of human muscle energy expenditure.," *Computer methods in biomechanics and biomedical engineering,* vol. 6, no. 2, pp. 99--111, 2003.
[21] T. K. Uchida, J. L. Hicks, C. L. Dembia, and S. L. Delp, "Stretching your energetic budget: how tendon compliance affects the metabolic cost of running," *PloS one,* vol. 11, no. 3, 2016.
[22] X. Zhou and A. Przekwas, "A fast and robust whole-body control algorithm for running," *International Journal of Human Factors Modelling and Simulation,* vol. 2, no. 1, pp. 127--148, 2011.
[23] X. Zhou and X. Chen, "Design and Evaluation of Torque Compensation Controllers for a Lower Extremity Exoskeleton," *ArXiv preprint arXiv:1907.02200,* 2019.